engineering proceedings

MDPI

Proceeding Paper

Addressing the Potential of L5/E5a Signals for Road ITS Applications in GNSS-Harsh Environments †

Amarildo Haxhi *, Manos Orfanos, Harris Perakis and Vassilis Gikas

School of Rural, Surveying and Geoinformatics Engineering, National Technical University of Athens, 9 Iroon Polytechneiou Str., 157 80 Zographos, Attic, Greece; orfanos_emmanouhl@mail.ntua.gr (M.O.); hperakis@central.ntua.gr (H.P.); vgikas@central.ntua.gr (V.G.)
* Correspondence: a_haxhi@mail.ntua.gr
† Presented at the European Navigation Conference 2023, Noordwijk, The Netherlands, 31 May–2 June 2023.

Abstract: This study explores the potential of satellite signals L5, E5a and B2a tracked by contemporary Android smartphones. Particularly, the objective is to investigate their performance capabilities and vulnerabilities concerned with L1, E1 and B1 bandwidths and a focus on land vehicle ITS (Intelligent Transportation Systems) applications aiming to address low to medium PVT (Positioning, Velocity and Timing) solutions. In this regard raw, kinematic GNSS measurements from two Android smartphones were collected (Xiaomi Mi 8 and One Plus Nord 2 5G) under GNSS-harsh environments. The Single Point Positioning (SPP) technique was adopted for processing the single-frequency, multi-constellation raw GNSS measurements through an Extended Kalman Filter (EKF). The results obtained indicate the benefits and difficulties of exploiting modernized GNSS signals for road ITS applications.

Keywords: GNSS raw measurements; Single Point Positioning; L5/E5a/B2a signals; multipath; Intelligent Transportation Systems

1. Introduction

With the release of Android Nougat in August 2016, the raw GNSS measurements on L1 (1575.42 MHz) became available to users on an increasing number of low-cost devices. Since then, research from various centers worldwide have tested and analyzed the performance capability of their properties including the satellite elevation angle, the received C/N0 (Carrier-to-Noise density ratio), the measurement accuracy with respect to high grade receivers, the sensitivity to cycle slips and multipath [1]. Published results [1] have pointed out that GNSS measurements on the L1 frequency are C/N0 dependent, featuring values approx. 10 dBHz less than those from high-grade receivers, suggesting that the adoption of C/N0 weighting schemes being a more appropriate approach. Concerning the satellite signal multipath, it was demonstrated that GNSS measurements on L1 are affected more severely than those in high grade receivers, especially in GNSS-harsh environments [1]. However, the main challenge for the quality of the GNSS measurement is that the embedded GNSS antenna in the smartphones lead to L1 pseudorange accuracies of the order of 4–5 m [2].

Following these developments, an increasing number of smartphones featuring dual-frequency capabilities was developed. Concerning L5, E5a and B2a, all three signals can be tracked from the GPS, Galileo and BeiDou satellites, respectively. L5/E5a/B2a signals are superior to L1/E1/B1 ones as a result of their design specifications [1,3]. For example, the chipping rate of L5/E5a/B2a's is higher than that of the L1/E1/B1 leading to more precise measurements. The lower level of observation noise in the code observables and their resilience against the multipath for GPS/Galileo/BeiDou L5/E5a/B2a signals has been validated through field surveys using various smartphones [1]. Contrarily, fever satellites are

check for updates

Citation: Haxhi, A.; Orfanos, M.; Perakis, H.; Gikas, V. Addressing the Potential of L5/E5a Signals for Road ITS Applications in GNSS-Harsh Environments. *Eng. Proc.* **2023**, *54*, 11. https://doi.org/10.3390/ENC2023-15430

Academic Editors: Tom Willems and Okko Bleeker

Published: 6 December 2023

being tracked on L5/E5a/B2a than on L1/E1/B1, whilst featuring lower C/N0 values. However, the rapid expansion of the European Galileo and BeiDou systems and the modernization of GPS raise the number of satellites (>60) transmitting on L5/E5a/B2a signals.

In this evolving landscape, this study aims to address the capabilities of L5/E5a/B2a signals in GNSS-harsh environments with a focus on land vehicle ITS applications requiring meter-level accuracy [4–6]. The structure of the paper is organized as follows. Firstly, the background and state of the art on L5/E5a/B2a signals is presented. Section 2 presents the methodology and fieldwork undertaken. The analysis of the raw GNSS measurements at the pre-processing and post-processing stage is presented in Section 3. Finally, Section 4 presents the key conclusions and discussion for future work.

2. Methods and Materials

2.1. Methods

Considering that the smartphone pseudorange measurements are characterized from high noise levels compared to high-grade geodetic GNSS receivers, at the pre-processing stage, they are smoothed using the Hatch filter [7,8].

$$\overline{p}_{r,k}^{s,S} = w p_{r,k}^{s,S} + (1-w)\left(\overline{p}_{r,k-1}^{s,S} + \varphi_{r,k}^{s,S} - \varphi_{r,k-1}^{s,S}\right)\overline{p}_{r,0}^{s,S} = p_{r,0}^{s,S} \quad (1)$$

where k, $k-1$ and 0 refer to the current, previous and initialization epochs accordingly, $p_{r,k}^{s}$ represents the pseudorange measurement, S indicates the GNSS system with $S \in (G : GPS,\ E : Galileo,\ C : BeiDou)$, s represents the satellite used, $\widetilde{p}_r^{s}$ is the smoothed pseudorange, φ_r^s is the precise but ambiguous carrier phase measurement and w is a weight factor that is inversely proportional to the number of consecutive epochs. To obtain and adapt a weighting value for w, a similar approach to [8] was adopted.

For computing the GNSS PVT solution, the Single Point Positioning (SPP) technique is implemented for the case of single-frequency, multi-constellation measurements [7]. The linearized equations for the observed minus computed single-frequency, multi-constellation pseudoranges is given as follows (the time notation t is omitted for simplicity): [7]:

$$E\left(\begin{bmatrix} \Delta\widetilde{\boldsymbol{p}}_{r,j}^{G} \\ \Delta\widetilde{\boldsymbol{p}}_{r,j}^{E} \\ \Delta\widetilde{\boldsymbol{p}}_{r,j}^{C} \end{bmatrix}\right) = \begin{bmatrix} \boldsymbol{G}_r^G & \boldsymbol{u}_{m_G} & 0 & 0 \\ \boldsymbol{G}_r^E & \boldsymbol{u}_{m_E} & \boldsymbol{u}_{m_E} & 0 \\ \boldsymbol{G}_r^C & \boldsymbol{u}_{m_C} & 0 & \boldsymbol{u}_{m_C} \end{bmatrix}\begin{bmatrix} \Delta\boldsymbol{r}_r \\ dt_{r,j}^{G} \\ ISB_{r,j}^{GE} \\ ISB_{r,j}^{GC} \end{bmatrix} \quad (2)$$

where $E(\cdot)$ denotes the expected operation, G, E and C are notations for the GPS, Galileo and BeiDou, respectively, r is the subscript for the receiver, j denotes the frequency used, m_S is the corresponding number of observations for each constellation and $\Delta\widetilde{\boldsymbol{p}}_{r,j}^{S}$ denotes the observed minus computed pseudoranges for each constellation $S \in (G, E, C)$. Also, $\boldsymbol{G}_r^S$ and $\boldsymbol{u}_{m_S}$ are the matrix containing the LOS (Line of Sight) unit directions vectors and the unit vector, respectively, for each constellation S, $\Delta\boldsymbol{r}_r$ is the receiver position vector, $dt_{r,j}^{G}$ is the receiver clock error with respect to GPS lumped with the receiver hardware delays, and $ISB_{r,j}^{GE}$ and $ISB_{r,j}^{GC}$ are the GPS-Galileo and GPS-BeiDou inter-system biases (ISB), respectively. The notation $\widetilde{\cdot}$ denotes that the observed pseudoranges are corrected for the orbit, clock, atmospheric delays, etc.

Another bias that should be handled appropriately refers to hardware delays that relate to the signals that the broadcasted satellite clock corrections are based on [7]. For example, the broadcasted satellite clocks of GPS satellites are based on the ionosphere-free (IF) linear combination (LC) of L1 + L2 frequencies, while for Galileo, they are based either on the IF LC of E1 + E5a or E1 + E5b frequencies. Instead, for the BeiDou system, the broadcasted satellite clock corrections refer to the B3 signal. Therefore, for the broadcasted satellite clocks ($dt^{s,S}$) to refer to the signals utilized in this study, the Timing Group Delay (TGD) and Broadcast Group Delay (BGD) should be applied for GPS/BeiDou and Galileo systems, respectively, as follows [7,9]:

$$dt^{s,G} - \frac{\mu_j^G}{\mu_1^G} TGD^s, \qquad j \in (1,5) \tag{3}$$

$$dt^{s,E} - \frac{\mu_1^E}{\mu_j^E} BGD^s_{E5a-E1}, \qquad j \in (1,5) \tag{4}$$

$$dt^{s,C} - TGD_1, \; for\ the\ B1\ signals \tag{5}$$

$$dt^{s,C} - TGD_{B2ap}, \; for\ the\ B2a\ signals \tag{6}$$

where μ_j^S is the frequency dependent coefficient, with $S \in (G : GPS, E : Galileo, C : BeiDou)$.

To estimate the PVT solution, the smartphone-based pseudorange and Doppler measurements are processed through an Extended Kalman Filter (EKF) [10]. The EKF algorithm was developed as an additional capability to the existing open-source software *PANGNAV 1.0.0* [10]. The EKF is described by

$$\boldsymbol{x}_{k|k-1} = f\left(\boldsymbol{x}_{k-1|k-1}\right) \tag{7}$$

$$\boldsymbol{P}_{k|k-1} = \boldsymbol{F}\boldsymbol{P}_{k-1|k-1}\boldsymbol{F}^{\boldsymbol{T}} + \boldsymbol{Q} \tag{8}$$

$$\boldsymbol{K}_k = \boldsymbol{P}_{k|k-1}\boldsymbol{H}^{\boldsymbol{T}}\left(\boldsymbol{H}\boldsymbol{P}_{k|k-1}\boldsymbol{H}^{\boldsymbol{T}} + \boldsymbol{R}_k\right)^{-1} \tag{9}$$

$$\boldsymbol{x}_{k|k} = \boldsymbol{x}_{k|k-1} + \boldsymbol{K}_k\left(\boldsymbol{z}_k - h\left(\boldsymbol{x}_{k|k-1}\right)\right) \tag{10}$$

$$\boldsymbol{P}_{k|k} = \boldsymbol{P}_{k|k-1} - \boldsymbol{K}_k\boldsymbol{H}\boldsymbol{P}_{k|k-1} \tag{11}$$

where the left indicator of $_{k|k-1}$ represents the current time instant whilst the right indicator represents the time instant value for the associated parameter being used, $\boldsymbol{x}_{k|k}$ is the state estimate at time k, $\boldsymbol{P}_{k|k}$ is the updated (a posteriori) estimate covariance at time k, $\boldsymbol{x}_{k|k-1}$ is the prediction of the state at time k, $\boldsymbol{P}_{k|k-1}$ is the predicted (a priori) estimate covariance at time k, $\boldsymbol{K}_k$ is the Kalman Gain at epoch k, $\boldsymbol{R}_k$ is the covariance of the measurement error at epoch k, $\boldsymbol{Q}$ is covariance of the process noise, $\boldsymbol{H}$ is the geometric matrix of the measurements (pseudorange and Doppler), h is the state-to-measurement mapping function, $\boldsymbol{F}$ is the state transition matrix, f is the state transition mapping function and $\boldsymbol{Z}_k$ is the measurement vector at epoch k. For the EKF, a constant velocity dynamic model was adopted, whilst the ISBs are handled as white noise [11].

2.2. Materials

In order to evaluate the impact of L5, E5a and B2a signals in GNSS-harsh environments for ITS applications, a kinematic experiment was carried out on 21 May 2022, at the NTUA campus and the greater area (Figure 1). The kinematic scenario's test trajectory was constructed such that the vehicle runs through sub-urban, urban and deep-urban areas (Figure 1). Table 1 contains information on the duration and length of each sub-trajectory.

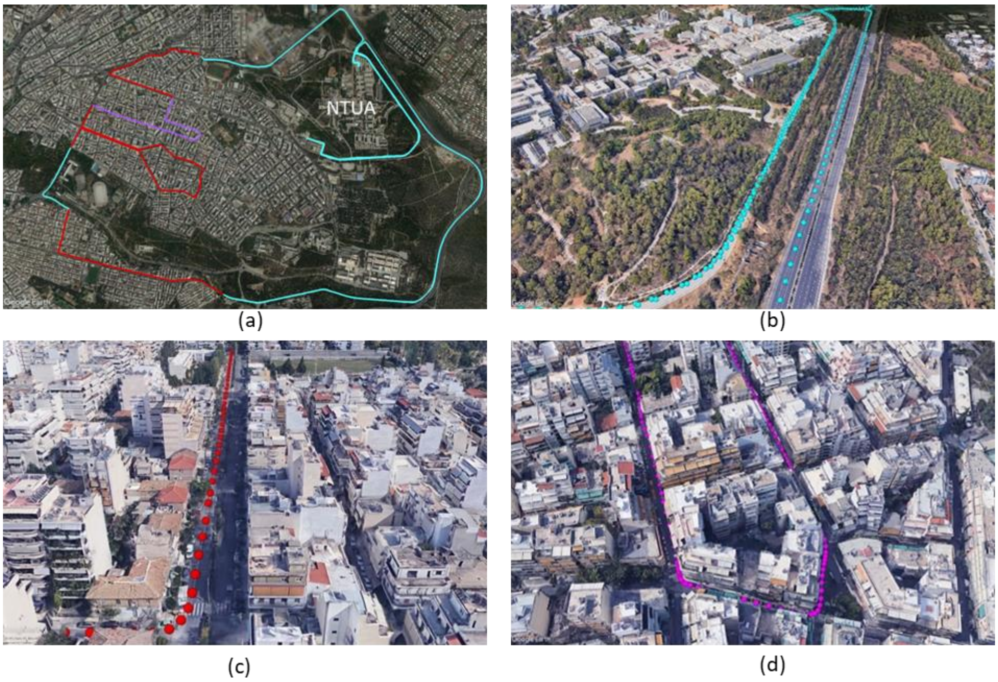

Figure 1. (**a**) Overall test trajectory which includes sub-urban (cyan), urban (red) and deep-urban (magenta) trajectories. (**b**) Sub-urban, (**c**) urban and (**d**) deep-urban environments.

Table 1. Characteristics of the total experimental trajectories and the underlying sub-trajectories.

Experimental Trajectory	Length (km)	Duration (min)
Sub-urban	9.62	21
Urban	5.35	17
Deep-urban	1.24	7
Total	16.21	45

Two separate datasets of spatio-temporal measurements were collected. The first one contains the raw GNSS measurements captured from two *Android* smartphones, the Xiaomi Mi 8 and the OnePlus Nord2 5G. Xiaomi Mi 8 is capable of tracking GPS, Galileo and BeiDou Signals on L1/L5, E1/E5a and B1, respectively. On the other hand, OnePlus Nord 2 5G can track L1/L5, E1/E5a and B1/B2a signals of GPS, Galileo and BeiDou, respectively. In order to realize an operational scenario, both smartphones were installed inside the vehicle, on the dashboard as shown in Figure 2. Finally, the GNSS raw measurements were retrieved from the smartphones using the *GNSSLogger* App [12].

The second dataset consists of the GNSS and IMU measurements collected from a tactical grade GNSS/IMU system (NovAtel® PwrPak7, iMAR IMU-FSAS) and a geodetic type GNSS antenna (Figure 2). The data from the tactical grade GNSS/IMU system were used to calculate the reference trajectory employing the PPK (Post Processed Kinematic) positioning technique. In this setup, the level arms among the various sensors mounted on the roof-top sensor platform and inside of the NTUA test vehicle are known thanks to the design specifications of the roof-top track. Furthermore, the level-arms among sensors are considered with respect to the IMU zero point.

Figure 2. (**a**) Roof-top sensor platform of the NTUA (National Technical University of Athens) test vehicle, (**b**) NovAtel® PwrPak7, (**c**) iMAR IMU-FSAS, (**d**) GNSS antenna, (**e**) Xiaomi Mi 8, (**f**) OnePlus Nord2 5G.

3. Analysis

3.1. Satellites' Visibility, C/N0 and Multipath

Figures 3 and 4 illustrate the performance of Xiaomi Mi 8 and OnePlus Nord 2 5G in terms of satellites being tracked and the received C/N0 values at specific frequency bands. For the Xiaomi Mi 8, 12, 9 and 11 satellites were being tracked for the GPS, Galileo and BeiDou systems on the L1, E1 and B1 bands, respectively. Regarding L5 and E5a, six GPS and nine Galileo satellites were tracked. OnePlus Nord 2 5G was able to track 12, 9 and 13 satellites for the GPS, Galileo and BeiDou systems on the L1, B1 and E1 bands, respectively. Finally, regarding L5, E5a and B2a, OnePlus Nord 2 5G was able to track eight GPS, nine Galileo and nine BeiDou satellites. The two smartphones have comparable tracking capabilities on L1/E1/B1, albeit OnePlus Nord 2 5G outperforms Xiaomi Mi 8 on the satellites being tracked on L5 for GPS.

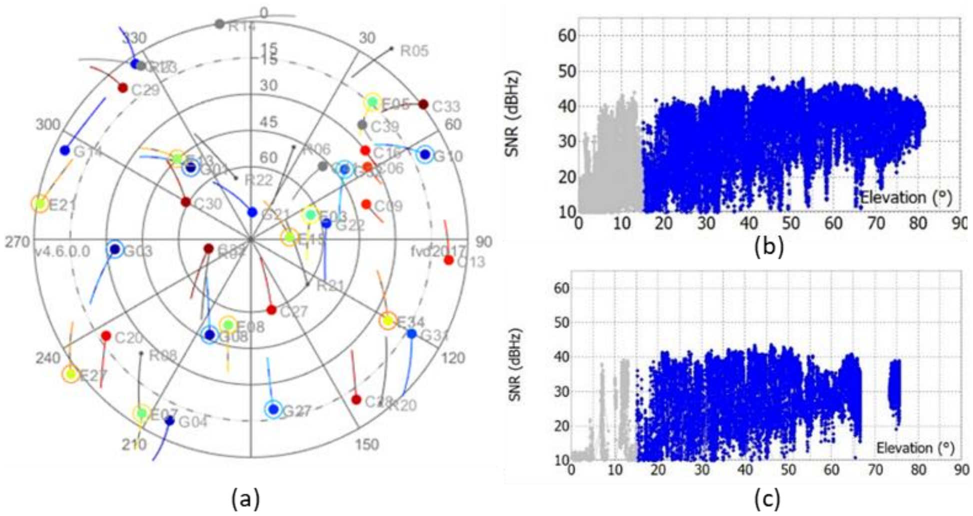

Figure 3. Xiaomi Mi 8: (**a**) Skyplot of the observed satellites on L1/E1/B1 (solid marks) and on L5/E5a (empty marks), (**b**) L1/E1/B1 and (**c**) L5/E5a/B2a C/N0 elevation-based (grey: elevation $\leq 15°$, blue: elevation > 15°) series (modified from *GNSSAnalysisApp* and *RTKLIB*).

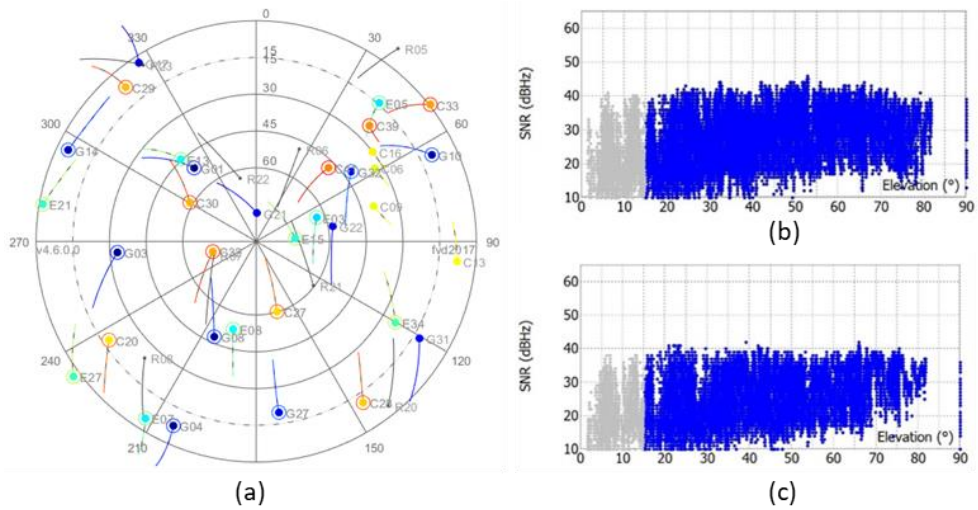

Figure 4. OnePlus Nord 2 5G: (**a**) Skyplot of the observed satellites on L1/E1/B1 (solid marks) and on L5/E5a (empty marks), (**b**) L1/E1/B1 and (**c**) L5/E5a/B2a C/N0 elevation-based (grey: elevation ≤ 15°, blue: elevation > 15°) series (modified from *GNSSAnalysisApp* and *RTKLIB*).

Data analysis reveals two points regarding the elevation-based C/N0 series obtained for the Xiaomi Mi 8 and OnePlus Nord 2 5G (Figures 3 and 4). Firstly, the C/N0 values of the L1/E1/B1 signals both for the Xiaomi mi 8 and the OnePlus Nord 2 5G seem not to depend on the satellite elevation angle, as opposed for the L5/E5a/B2a signals. As a result, in this study, an elevation-dependent weighting scheme is used for L5/E5a/B2a signals and a C/N0-dependent weighting scheme [10] is implemented for L1/E1/B1 signals. Moreover, one should notice that the C/N0 values for L1/E1/B1 signals are higher than those of L5/E5a/B2a ones. On the other hand, the C/N0 values of L5/E5a/B2a signals seem to be less-susceptible to abrupt changes than those observed for the L1/E1/B1 signals.

In this study, in order to assess the multipath effect on L1/E1/B1 and L5/E5a/B2a, we use the closed form expression for the dual-frequency ionosphere corrected CMC (Code-Minus-Carrier) linear combination [7,13]. According to Figure 5, the multipath for Xiaomi Mi 8 ranges between −5 m and 5 m for L1/E1 signals, while for the L5/E5a signals, it lies in the range of −2 m to 2 m. This discrepancy supports the hypothesis that L5/E5a signals are more resilient to multipath by design, compared to L1/E1 ones. Also, multipath is seen to affect the GPS and Galileo measurements in the same way, as the multipath-RMS values for L1-E1 and L5-E5a are relatively close. Regarding the different sub-trajectories, it seems that multipath has more or less the same effect on the pseudorange measurements, irrespective of the environment type. Nevertheless, excessive multipath is observed both for the urban and deep-urban sub-trajectories.

For OnePlus Nord 2 5G, a lower impact of multipath is noticed for L5/E5a/B2a signals compared to those of L1/E1/B1 signals (Figure 6). In numbers, the RMS values observed due to multipath for the L1, E1 and B1 are 1.43 m, 0.96 m and 0.89 m, respectively, while for L5, E5a and B2a, they equal 0.25 m, 0.22 m and 0.17 m, respectively. Based on these results, one can also infer that E1 and B1 signals are more resilient to multipath than the L1, whilst for the L5, E5a and B2a, a more comparable performance is evident. Similar remarks could be made for the sub-trajectories for the OnePlus Nord 2 5G, as those made for Xiaomi Mi 8.

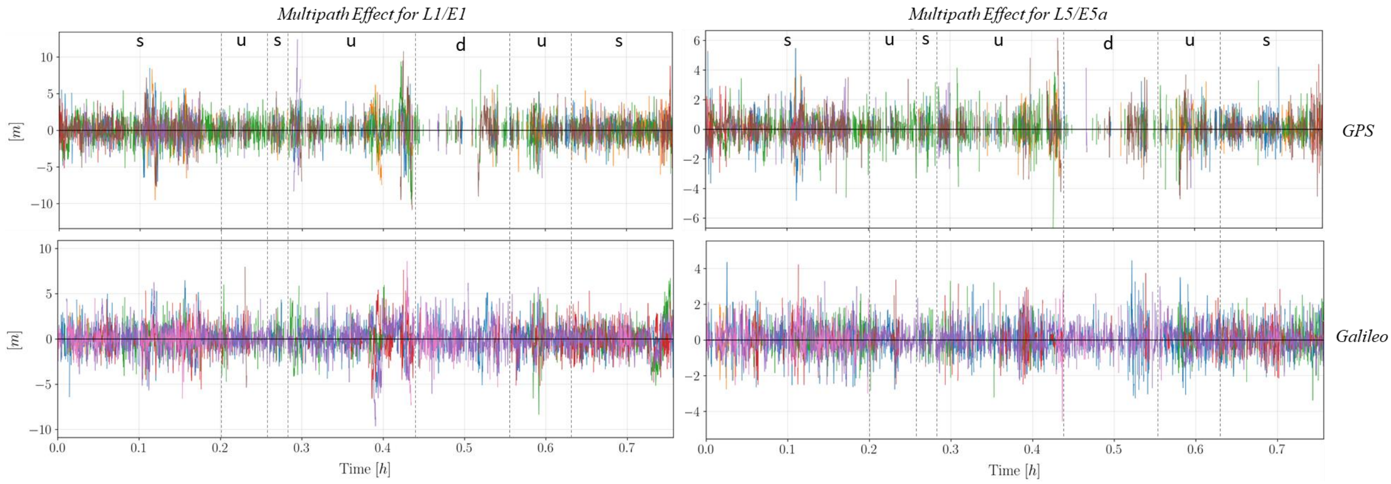

Figure 5. Multipath effect in meters (m) of L1/E1 and L5/E5a signals for Xiaomi Mi 8. The vertical dotted lines separate the intervals for each sub-trajectory, i.e., sub-urban (s), urban (u) and deep-urban (d). The different colors represent the GPS and Galileo satellites.

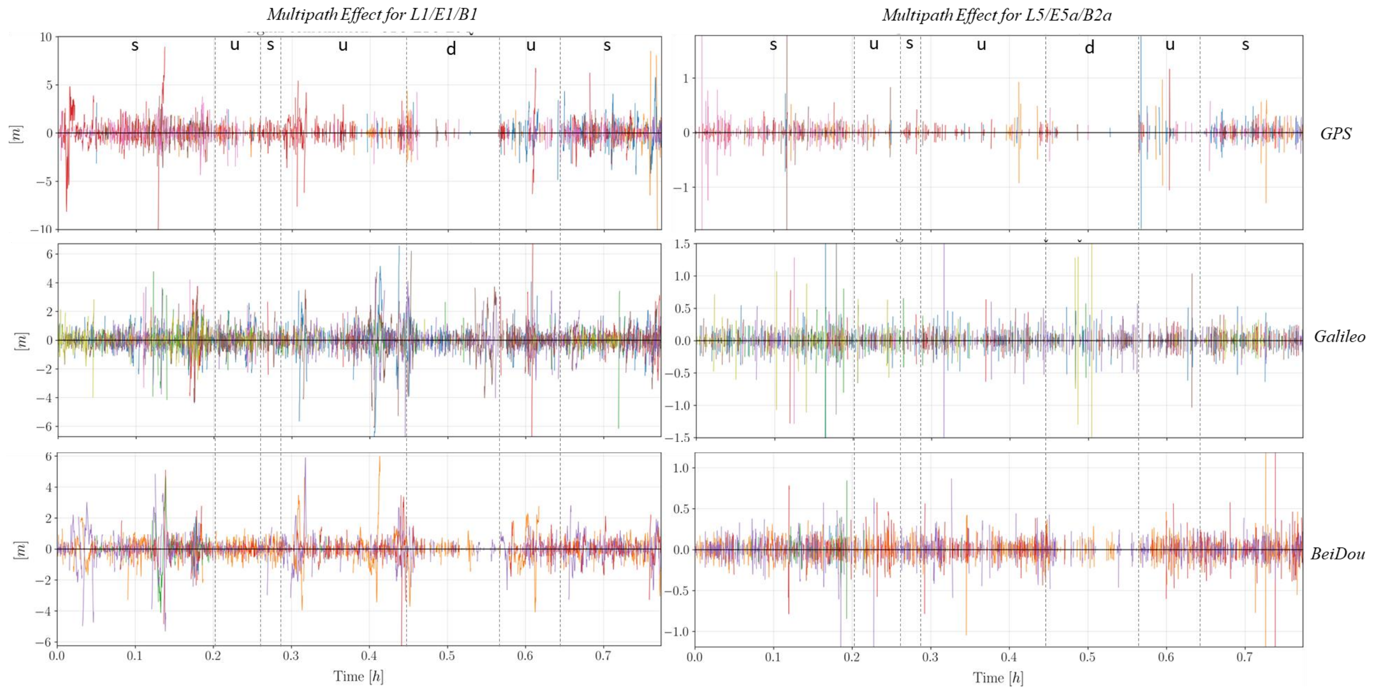

Figure 6. Multipath effect in meters (m) of L1/E1/B1 and L5/E5a/B2a signals for One Plus Nord 2 5G. The vertical dotted lines separate the intervals for each sub-trajectory, i.e., sub-urban (s), urban (u) and deep-urban (d). The different colors represent the GPS, Galileo and BeiDou satellites.

3.2. Accuracy of the PVT solution

The assessment of the PVT quality resides on measures of trueness (i.e., deviation from reference trajectory) and precision (i.e., repeatability). Table 2 summarizes the deviation (Root Mean Square, RMS) of the position solution for Xiaomi Mi 8 for the two sets of E1/L1/B1 and L5/E5a multi-constellation raw GNSS data.

Table 2. Horizontal position and velocity RMS errors of Xiaomi Mi 8 with respect to the reference trajectory.

Trajectories	Horizontal Position RMS (m)		Horizontal Velocity RMS (m/s)	
	L1/E1/B1	L5/E5a	L1/E1/B1	L5/E5a
Sub-Urban	2.9	3.5	1.4	1.7
Urban	5.3	6.8	1.5	1.8
Deep-Urban	6.6	7	1.6	2.0
Total	4.7	5.6	1.5	1.8

Clearly, concerning Xiaomi Mi 8, Table 2 indicates a better performance for the L1/B1/E1 position solution (RMS: 2.9 m) compared to the L5/E5a (RMS: 3.5 m). Furthermore, a horizontal RMS value of 2.9, 5.3 and 6.6 m is achieved for the sub-urban, urban and deep-urban trajectories, respectively. These results indicate the superiority of the estimated solution when multi-constellation GNSS measurements are used.

Two points are clearly evident concerning the L5/E5a solution no matter whether or not the accuracy obtained is significantly lower than that obtained for L1/E1/B1. Firstly, the Xiaomi MI 8 does not receive signals on B2a; therefore, more satellites are being monitored on the first frequency than on the second one. Secondly, this outcome is heavily affected by the poor observation geometry due to smartphone placement (dashboard).

In contrast, opposite conclusions result for the horizontal position errors obtained for the OnePlus Nord 2 5G (Table 3). For the case of L5/E5a/B2a solutions, the horizontal RMS errors improve by 21%, 17.1%, 14.7% and 22.5% for the total, sub-urban, urban and deep-urban trajectories, respectively, with respect to the L1/E1/B1 solution. This improved performance is due to the superior precision of the GNSS measurements on L5/E5a/B2a bands when compared to the L1/E1/B1 counterparts. Furthermore, as already stated, the One Plus Nord 2 5G is capable of receiving an extra signal (i.e., B2a) compared to Xiaomi Mi 8, which allows for tracking more satellites on the second frequency. Finally, it is worth noting that the tuning process of OnePlus Nord 2 was not as straightforward as that for Xiaomi Mi 8, indicating that better or more advanced filter tuning could potentially lead to superior results for the OnePlus Nord 2 5G.

Table 3. Horizontal position and velocity RMS errors of OnePlus Nord 2 with respect to the reference.

Trajectories	Horizontal Position RMS (m)		Horizontal Velocity RMS (m/s)	
	L1/E1/B1	L5/E5a/B2a	L1/E1/B1	L5/E5a/B2a
Sub-Urban	6.0	4.7	2.5	2.0
Urban	6.2	4.8	1.8	1.5
Deep-Urban	6.8	5.8	1.9	1.8
Total	6.2	4.9	2.1	1.7

In terms of horizontal velocity errors, both smartphones perform in a precision range of a few m/s (Tables 2 and 3). This performance could be attributed to the low precision of the Doppler-shift measurements acquired from *Android* devices [14]. The Xiaomi Mi 8 performs best when L1/E1/B1 measurements are employed, resulting in an accuracy of 1.5 m/s over the whole experimental trajectory. Regarding OnePlus Nord 2, comparing the L5/E5a/B2a signal velocities to the L1/E1/B1 ones, an improvement of 19%, 20%, 16.7% and 5% is noted for the complete, sub-urban, urban and deep-urban trajectories.

4. Conclusions

In this study, the performance capabilities of the raw GNSS measurements on L5/E5a/B2a signals from *Android* devices is investigated for road ITS applications. Specifically, a representative dataset was created by collecting GNSS raw measurements from two *Android* smartphones, namely, the Xiaomi Mi 8 and OnePlus Nord 2 5G, under GNSS-harsh environments. The raw GNSS pseudoranges obtained on L1/E1/B1 and L5/E5a/B2a were smoothed using a Hatch-Filter and processed through an EKF filter algorithm for computing the estimated PVT solution. In addition, the Doppler-shift measurements derived from the *Android* devices were integrated into the EKF filter. The PVT solutions for L1/E1/B1 and L5/E5a/B2a were compared against a reference PPK trajectory produced from high-grade navigation equipment and software.

Data analysis revealed that both smartphones used in this study track more satellites on L1/E1/B1 signals than on L5/E5a/B2a. Additionally, a slight improvement in the tracking capabilities has been observed for the most recently released device (i.e., OnePlus Nord 2 5G) for the L5/E5a/B2a signals compared to Xiaomi Mi 8. Furthermore, data collection on the L1/E1/B1 seems to exhibit higher C/N0 values, compared to those for L5/E5a/B2a; however, abrupt changes occur more frequently irrespective of the satellite's elevation. Contrariwise, measurements on L5/E5a/B2a tend to exhibit lower C/N0 values, but with fewer abrupt changes, which however relate to an increase in the satellite view angle. In terms of multipath, the investigation shows that pseudorange measurements on L5/E5a/B2a signals are more robust than those obtained on L1/E1/B1.

Regarding the PVT performance, the results obtained for both devices collecting data on the L5/E5a/B2a signals are promising. In particular, for Xiaomi Mi 8, even though the PVT solution refers to only L5/E5a measurements, it achieves a comparable performance with that of L1/E1/B1, in terms of horizontal position and velocity errors. On the contrary, for the case of L5/E5a/B2a signals, the PVT solution for the OnePlus Nord 2 5G shows a significant improvement when compared to the PVT solution for L1/E1/B1 signals.

In order to further improve the PVT solution, it is proposed that future work will focus on the single differences between satellites as the basic functional model. In this approach, it is foreseen that receiver specific biases should be mitigated to a great extent, and therefore, a better performance of the Hatch-Filter should be realized [8]. Also, a range of additional, contemporary smartphones shall be tested, as in the experiment conducted in this paper, a Record and Replay system (Racelogic's LabSat 3 Wideband) was utilized.

Author Contributions: Conceptualization, A.H., H.P. and V.G.; methodology, A.H.; software, A.H.; validation, A.H. and V.G.; formal analysis, A.H.; investigation, A.H., M.O., H.P. and V.G.; resources, A.H.; data curation, A.H.; writing—original draft preparation, A.H.; writing—review and editing, A.H. and V.G.; visualization, A.H.; supervision, V.G. All authors have read and agreed to the published version of the manuscript.

Funding: This research has been co-financed by the European Regional Development Fund of the European Union and Greek national funds through the Operational Program Competitiveness, Entrepreneurship and Innovation, under the call RESEARCH–CREATE–INNOVATE (project code:T2EDK-03966).

Institutional Review Board Statement: Not applicable.

Informed Consent Statement: Not applicable.

Data Availability Statement: Data supporting the reported results can be accessed by contacting the authors at a_haxhi@mail.ntua.gr.

Conflicts of Interest: The authors declare no conflict of interest.

References

1. Zangenehnejad, F.; Gao, Y. GNSS smartphones positioning: Advances, challenges, opportunities, and future perspectives. *Satell. Navig.* **2021**, *2*, 24. [CrossRef] [PubMed]
2. Bahadur, B. A study on the real-time code-based GNSS positioning with Android smartphones. *Measurement* **2022**, *194*, 111078. [CrossRef]
3. Miao, W.; Li, B.; Gao, Y. The Superiority of Multi-GNSS L5/E5a/B2a Frequency Signals in Smartphones: Stochastic Modeling, Ambiguity Resolution, and RTK Positioning. *IEEE Internet Things J.* **2023**, *10*, 7315–7326. [CrossRef]
4. GSA. Report on Road User Needs and Requirements Outcome of the European GNSS' User Consultation Platform. Jan. 2019. Available online: https://www.euspa.europa.eu/gnss-applications/user-needs-and-requirements (accessed on 5 June 2023).
5. Clausen, P.; Gilliéron, P.; Perakis, H.; Gikas, V.; Spyropoulou, I. Assessment of Positioning Accuracy of Vehicle Trajectories for Different Road Applications. *IET Intell. Transp. Syst.* **2017**, *11*, 113–125. [CrossRef]

6. Haxhi, A.; Perakis, H.; Gikas, V.; Fafoutellis, P.; Mantouka, E.; Vlahogianni, E.I.; Pnevmatikou, A.; Fortsakis, P. Towards Smartphone-based Enhanced GNSS Positioning for Eco Driving ITS Services. In Proceedings of the 10th International Congress on Transportation Research, Rhodes, Greece, 2–3 September 2021.
7. Teunissen, P.J.G.; Montenbruck, O. (Eds.) *Springer Handbook of Global Navigation Satellite Systems*; Springer International Publishing: Cham, Switzerland, 2017. [CrossRef]
8. Geng, J.; Jiang, E.; Li, G.; Xin, S.; Wei, N. An Improved Hatch Filter Algorithm towards Sub-Meter Positioning Using only Android Raw GNSS Measurements without External Augmentation Corrections. *Remote Sens.* **2019**, *11*, 1679. [CrossRef]
9. Romero, I. *The Receiver Independent Exchange Format Version 4.00*; IGS: Pasadena, CA, USA, 2021.
10. Haxhi, A.; Perakis, H.; Mpimis, T.; Gikas, V. Testing of a Combined Hatch Filter/RAIM Algorithm for SPP Smartphone Kinematic Positioning in GNSS Harsh Environments. In Proceedings of the 2nd Symposium of IAG Commission 4 "Positioning and Applications, Potsdam, Germany, 5–8 September 2022. [CrossRef]
11. Petovello, M. *GNSS Solutions: Calculating Time Offsets*; InsideGNSS: Red Bank, NJ, USA, 2013.
12. GnssLogger App—Apps on Google Play. Available online: https://play.google.com/store/apps/details?id=com.google.android.apps.location.gps.gnsslogger&hl=en&gl=US (accessed on 23 October 2022).
13. Aarnes, P.H. GNSS Multipath Analysis. 5 May 2023. Available online: https://github.com/paarnes/GNSS_Multipath_Analysis_Software (accessed on 16 May 2023).
14. Ramesh, A.; Renaudin, V.; Ragoin, C.; Ortiz, M. External-Connection Free, Accurate Standalone GNSS Positioning on Smartphones. In Proceedings of the Positioning and Navigation for Intelligent Transport Systems POSNAV, Berlin, Germany, 3–4 November 2022.